ACS Photonics

Article

pubs.acs.org/journal/apchd5

Reversible Optical Switching of Infrared Antenna Resonances with Ultrathin Phase-Change Layers Using Femtosecond Laser Pulses

Ann-Katrin U. Michel,[†] Peter Zalden,[‡,§] Dmitry N. Chigrin,[†] Matthias Wuttig,[†,∥] Aaron M. Lindenberg,[‡,§,⊥] and Thomas Taubner*[,†,∥]

[†]I. Institute of Physics (IA) and [∥]JARA – Fundamentals of Future Information Technology, RWTH Aachen University, 52056 Aachen, Germany

[‡]Stanford Institute for Materials and Energy Sciences, SLAC National Accelerator Laboratory, Menlo Park, California 94025, United States

[§]PULSE Institute, SLAC National Accelerator Laboratory, Menlo Park, California 94025, United States

[⊥]Department of Materials Science and Engineering, Stanford University, Stanford, California 94305, United States

Supporting Information

ABSTRACT: Recently, phase-change materials (PCMs) have gained a lot of interest in the field of active metamaterials and plasmonics due to their switchable optical properties. In the infrared spectral range the huge contrast in the refractive index between an amorphous and a crystalline phase can be employed for nonvolatile tuning of nanoantenna or metasurface resonances. To make use of such concepts in devices, the reversible switching of the active material has to be realized. Here we demonstrate such reversible cycling by applying femtosecond pulses from a Ti:sapphire laser. These optical pulses trigger the phase transitions of the PCM thin film, which is covering infrared nanoantennas. $Ge_3Sb_2Te_6$ is chosen as the PCM, since it offers very low losses in the infrared spectral range. The layer geometry presented is exceptionally thin (~1/50 of the operating wavelength) and the design intentionally avoids lossy capping layers. Infrared reflectivity measurements verify the laser-induced resonance shifts of the plasmonic nanoantenna arrays. This switching mechanism opens the possibility to optically perform active, reversible, and nonvolatile tuning of metasurfaces.

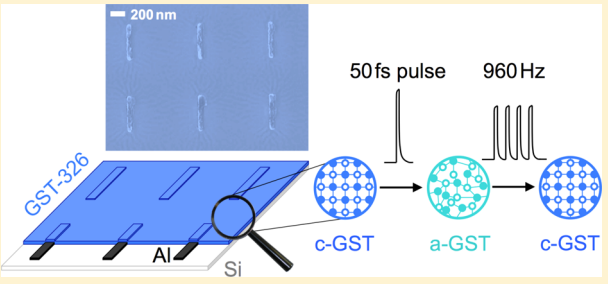

KEYWORDS: *active nanooptics, nanoantennas, resonance tuning, phase-change materials, reversible switching, active plasmonics*

In the field of plasmonics and nanophotonics, many investigations have focused on passive devices based on metallic nanostructures. Regarding the development of these metallic nanostructures, tremendous progress has been achieved in the last years upon introducing planar, ultrathin metamaterials, so-called metasurfaces (MSs). They surpass electromagnetic properties of natural solids, enabling for example negative refractive index, efficient light concentrators or magnetism in the visible range.[1] The parameters of the nanostructures, such as geometry and material, determine their optical properties, which are usually achieved in a resonant way at a specific wavelength.

However, an actively tunable resonance is required for applications,[2] for example, for chemical sensing[3] or the active control of signals in optoelectronics.[4] The modulation of the structure's resonance frequency can be realized either by damping the resonance amplitude or by shifting the position of the resonance frequency. Different approaches to influence the resonance frequency of plasmonic nanoantennas and split-ring resonators have been presented, for example, by influencing the coupling of the nanostructures[5] or by varying the antenna thickness.[6] By using new material platforms and designing hybrid systems consisting of nanostructures and functional dielectrics or semiconductors,[7] resonance frequency shifting has been achieved in many different ways, for example, by reorientation of nematic liquid crystals covering a metasurface,[8] by changing the carrier concentration of doped indium antimony[9] or graphene,[10] by exploiting the metal-to-insulator transition of vanadium dioxide, which accompanies the structural transition,[11] or by using metal hydrides.[12−14]

In this paper, we use a group of chalcogenides, named phase-change materials (PCMs), to shift the resonance frequency of nanoantenna arrays. PCMs are a particularly promising candidate to realize modulation functionality, since they allow for ultrafast reversible switching between its temperature stable structural phases. PCMs,[15−17] which are typically based on the combinations of the elements germanium, antimony, tellurium, and indium, show a pronounced change of their dielectric function $\varepsilon(\omega)$ during the structural phase transition between the amorphous and the crystalline states.[18] In the mid-infrared spectral range, PCMs offer a huge contrast in the real part of

Received: April 15, 2014
Published: August 21, 2014

the permittivity ε_1. Furthermore, they also possess a very small ratio of the imaginary to the real part of the permittivity, that is, $\varepsilon_2/\varepsilon_1 \ll 0.1$, which corresponds to very low losses due to absorption.[19]

With this combination of properties, PCMs are of great interest for the design of metamaterials and in the field of tunable plasmonics and nanooptics.[20−26] It has been shown recently that antenna devices based on $Ge_3Sb_2Te_6$[27] allow low-loss, wide-range tuning of antenna resonances in the mid-infrared spectral range.[19] Advantageously, PCMs offer the possibility for nonvolatile resonance tuning in contrast to vanadium dioxide VO_2. The temperature-dependent insulator-to-metal transition in VO_2 has been utilized for nanostructure resonance tuning.[11,6,28]

To further demonstrate the potential of PCMs for application as plasmonic devices, their properties must be cyclable in a repetitive way on short time scales. It is well-known that the structural rearrangement in phase-change materials can be triggered by electrical[29] or optical[30] pulses, which has enabled the design of optical (e.g., DVD-RW[31]) and nonvolatile electronic memory devices (e.g., PCRAM[32]).

Here we report femtosecond laser-induced switching of infrared nanoantenna resonances by using a thin film of the PCM $Ge_3Sb_2Te_6$ (from here on abbreviated as GST-326). The successful switching is probed by Fourier-transformed infrared (FTIR) spectroscopy of the bare GST-326 thin film, as well as of the nanoantenna arrays covered with GST-326. In contrast to the sample geometry presented in other publications showing optical switching of PCMs with nanosecond pulses,[30,33] the present layer stack is extremely thin (~1/50 of the operating wavelength compared to ~1/6 in ref 33) and does not include absorbing capping layers.[34] Such capping layers would introduce additional losses in the optical device and decrease the achievable resonance shift by increasing the distance between the nanostructure and the PCM layer.

Figure 1A shows a schematic cross-section of an antenna array. Aluminum nanoantennas of about 35 nm height are

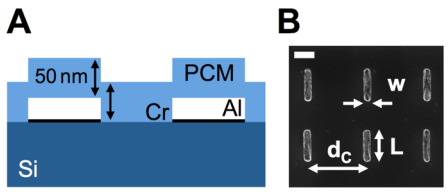

Figure 1. (A) Schematic drawing (not to scale) of the sample cross-section including aluminum nanoantennas (35 nm height including a 3 nm adhesive chromium layer beneath) covered by 50 nm GST-326 (bright blue) on a silicon substrate (dark blue). (B) SEM image of aluminum nanoantennas with width w, length L, and distance d_C (here, w = 100 nm and L = 500 nm). Scale bar: 300 nm.

covered with 50 nm amorphous GST-326. Single aluminum nanoantennas exhibit a rather broad infrared resonance. In order to perform an effective switching of an antenna array response, it is instructive to design an array with as narrow resonances as possible. To achieve this goal, we rely on the wood anomaly effect.[35] In a lattice of resonant scatterers an interference between scatterer resonance and Bragg resonances of the lattice results in narrow resonances of the combined system.

In other studies, gold is often used for plasmonic nanoantennas.[24,25,33] In our sample layout, the phase-change layers are in direct contact with the nanorods as shown in Figure 1A. Strong gold diffusion into the PCM layer during thermal crystallization justifies the use of aluminum as an alternative nanoantenna material, since negative bonding enthalpy has been found for AuX_2 compounds (X = In and Sb, for example).[36] Furthermore, aluminum in plasmonics has a high potential regarding industry compatibility since it is the most commonly used metal in silicon-based very-large-scale integration (VLSI).[37]

The antenna array resonance position is determined by the antenna geometry and the chosen materials for the antennas, the substrate and the cover layer. Changing the structural phase of the GST-326 cover layer shifts the spectral position of the antenna array's resonance, since the permittivity $\varepsilon(\omega)$ of the GST-326 changes. In the investigated spectral range, the refractive index is changing from about 3.58 in the amorphous to about 6.33 in the crystalline phase.[38] Crystallization or an increase of the refractive index of the GST-326 cover layer, respectively, results in a shift of the antenna resonances to smaller wavenumbers. In our earlier work,[19] we have recently demonstrated that antenna resonances can be tuned by using this low-loss PCM. There, the resonance shift was only possible in one direction (amorphous to crystalline), since the phase-change was achieved using a thermal hot plate. In the present study, the reversible optical switching is realized with femtosecond laser pulses. The incorporation of switchability into MS systems is a crucial point in the development of novel, ultrathin devices.[1,4]

In Figure 2A, a detailed scheme of the sample treatment is shown. First the as-deposited amorphous AD-GST-326 layer, which is covering the entire sample, is thermally transformed into the crystalline C-GST-326 phase. To achieve the reversible switching of the antenna array resonances (from C- to melt-quenched MQ-GST-326 and from MQ- to recrystallized RC-GST-326), a femtosecond laser source with 800 nm (12500 cm^{-1}) central wavelength has been used. Arrays with antennas of length L = 400 and 500 nm, have been switched independently. To achieve different phases of the GST-326 layer, the antenna arrays have been optically reamorphized into the MQ phase and one of them has finally been recrystallized (into RC). As a result, spectra of two identical arrays with two different cover layers (MQ- and RC-GST-326) can be investigated with the FTIR microscope.

The specific experimental parameters are displayed in Figure 2B. The two fundamental phase transformations—amorphization and recrystallization—take place on different temperature and time scales.[39] In this article we focus on reversible switching, employing an optically triggered phase-change, which will be discussed in detail. The parameters for thermal crystallization can be found in our earlier work.[19]

To amorphize the crystalline GST-326 layer, the crystal lattice has to be molten and subsequently quenched to room temperature to avoid any recrystallization of the atomic structure. A 50 fs single pulse of the femtosecond laser with a relatively high fluence of 51 mJ/cm^2 is sufficient to induce amorphization from C- to MQ-GST-326 phase. During the amorphization process, the fs laser introduces a very high density of electron hole pairs in the sample, which relax by electron—phonon coupling and melt the PCM. The subsequent fast cooling quenches the melt into the amorphous (glassy) phase of the thin film.

For inducing the crystallization process (MQ to RC) a temperature below the melting temperature T_M (ca. 640 °C[40]),

dx.doi.org/10.1021/ph500121d | ACS Photonics 2014, 1, 833−839

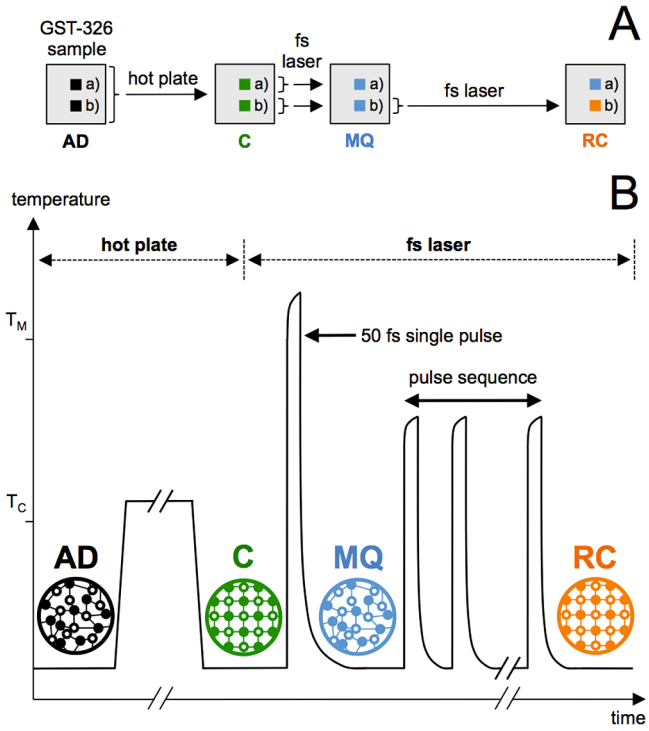

Figure 2. (A) Sample scheme: the GST-326 on top of the identical antenna arrays (a) and (b) is in the as-deposited, amorphous phase (AD). First, it is thermally crystallized (C) and hereafter optically reamorphized into the melt-quenched state (MQ). Finally array (b) is recrystallized (RC) by fs laser pulses. (B) AD-GST-326 is annealed above the crystallization temperature T_C (160 °C[42]) to change to C-GST-326. For reamorphization it needs to be heated above the melting temperature T_M (ca. 640 °C[41]). This is triggered by a single ultrafast laser pulse. Subsequent quenching leads to the melt-quenched state MQ-GST-326. For the recrystallization process, for which a temperature between T_C and T_M is necessary, the fs laser is set to repetitive pulsing at 960 Hz.

but above the crystallization temperature T_C (160 °C[41]), is necessary. Furthermore, the crystal lattice of the GST-326 film needs time to relax from its amorphous to its crystalline state, which leads to a relatively long duration of the phase transformation compared to the time needed to melt-quench the lattice into an amorphous state (C to MQ). Repetitive excitation can also provide sufficient overall time to recrystallize the material, which has been shown in recent reports; for example, see ref 42. Using a sequence of correlated pulses, each shorter than 1 ps, a smaller fluence is necessary.[42,43] Indeed, running the laser for 1 s in a repetitive mode (960 Hz) with a fluence of about 31 mJ/cm^2 per 50 fs pulse completed the recrystallization.

These fluences of the fs laser pulses have been chosen to achieve complete phase transformations for the GST-326 layer, according to the FTIR spectra of bare GST-326 thin films as displayed in Figure 3. There, a GST-326 thin film (no antennas) has been characterized. The spectra for AD- and MQ-GST-326, as well as for C- and RC-GST-326, are nearly identical, which confirms that the material after the laser-induced switching resembles the initial phases after thermal annealing.

In Figure 4 the antenna array reflectance spectra probed by FTIR microscopy are displayed. All spectra have been normalized to bare GST-326 thin films, as shown in Figure 3.

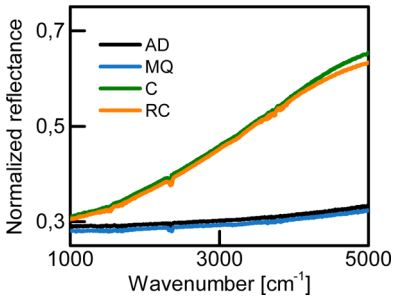

Figure 3. Experimental data for a thin film of GST-326 (without antennas) in all investigated structural phases AD, C, MQ, and RC, measured with an FTIR microscope aperture of about (20 × 20) μm^2 unpolarized incident light and normalized to a gold mirror. These spectra prove the structural state of the GST-326-amorphous (AD, MQ) and crystalline (C, RC) . The color code is in accordance with Figure 2.

The columns A and B correspond to different antenna lengths L, which are 500 nm for column A and 400 nm for column B. Furthermore, the reflectance spectra are divided into different panels to differentiate between the sample treatments: spectra for the GST-326 layer in its as-deposited (AD) and annealed phase (C) are shown in panel 1, whereas in panel 2 the reflectance spectra for both GST-326 phases after laser-induced phase transition (MQ- and RC-GST-326) are displayed.

The strong maximum of each spectrum results from the resonance of the investigated antenna array. The resonance peaks of the antenna arrays covered with crystalline GST-326 are shifted to smaller wavenumbers relative to the amorphous GST-326 phase, since the refractive index is increased.

The shift of the antenna resonance position due to the thermal heating from the as-deposited amorphous (AD) into the crystalline (C) phase of the cover layer is marked as the shift of the resonance peak 1 → 2 in panel 3 of Figure 4. In contrast, the shifts of the resonance peaks 2 → 3 and 3 → 4 are all triggered optically using a femtosecond laser source. These changes in the resonance position mark reversible shifts, which correspond to reamorphization and recrystallization of the GST-326 cover layer, respectively. For the rearmophization, the crystalline GST-326 is transformed into the melt-quenched (MQ) amorphous phase, marked as a shift of the resonance position 2 → 3. Thereafter, this MQ state of the cover layer is tranformed into the recrystallized (RC) phase again, which is displayed as peak shift 3 → 4. The achieved resonance shifts are quantified via a tuning figure of merit (FOM), which is the ratio between the resonance shift and fwhm of the antenna resonance. A tuning FOM of up to 0.86 can be determined, which is huge compared to literature, where FOM of up to 0.68 have been reported.[20,33]

Moreover, a significant advantage of the fs laser switching scheme as compared to ns diode lasers which are commonly used for switching the phase of the PCM in,[33,38] is the possibility to induce the phase change without the need of thermal barriers between the PCM and the substrate. Commonly, PCMs are amorphized by laser-induced thermal melting of the PCM on the substrate. A steady-state heat flow between the liquid PCM and the substrate has to be established. In the absence of a thermal barrier between the two layers, it requires very high laser powers for thermal heating with ns laser pulses. In contrast, processes typical for fs laser mechanisms are not limited by the requirement for steady state conditions and allow switching the PCM layer in the present

dx.doi.org/10.1021/ph500121d | ACS Photonics 2014, 1, 833−839

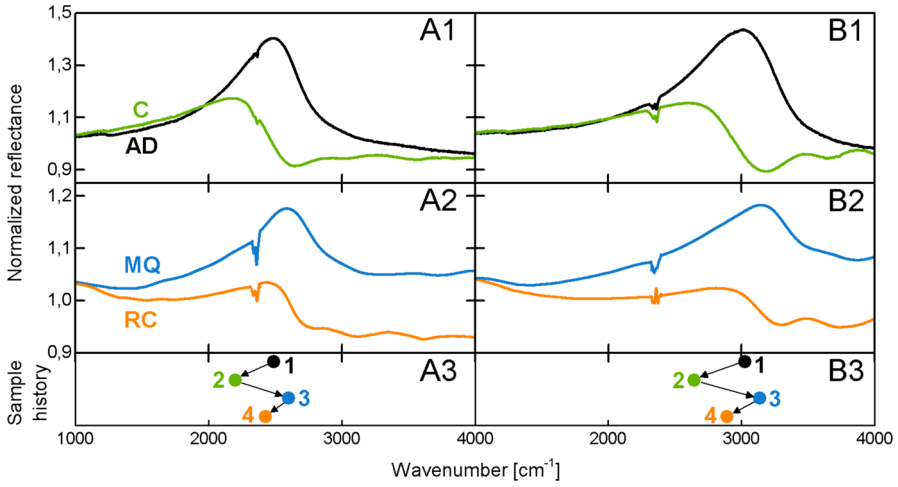

Figure 4. Experimental reflectance spectra for aluminum nanoantennas below a 50 nm GST-326 layer, measured with an FTIR microscope aperture of (20 × 20) μm^2, normalized to a GST-326 thin film. The incident light is polarized along the antennas. In (A), the length of the nanoantennas is 500 nm, which in (B) is 400 nm. The FTIR microscope aperture includes about 400 antennas for L = 500 nm (A) and about 625 antennas for L = 400 nm (B). The reflectance spectra for the optically melt-quenched (MQ) GST-326 are shown in blue. The spectra for the optically recrystallized (RC) GST-326 are displayed in orange. For comparison, in A1 and B1, the spectra for the antenna arrays covered with as-deposited (AD, black) and crystallized (C, green) GST-326 are depicted.[14] In panels 3, all resonance peak positions of the antenna arrays are compared in their chronological order, from AD = 1 to RC = 4, in accordance with the color code used in the other viewgraphs. The small absorption peak at about 2350 cm^{-1} is due to atmospheric CO_2 absorption.

configuration without a thermal barrier. This enables ultrathin sample geometries. Furthermore, it enables strong antenna resonance shifts, since damping due to very absorptive thermal barriers can be excluded. Additionally, a protective capping layer on top of the antennas (below the GST-326 layer) would introduce a distance between the antennas and the PCM. As a result, the change of the refractive index caused by switching from amorphous to crystalline GST-326 would have less influence on the antennas compared to a sample layout as used in the presented work. Finally, this would lead to a decreased resonance frequency shift.

With the described laser parameters, reproducible and reversible optical switching of antenna array resonances has been achieved. Nevertheless, the antenna resonance positions with the cover layers of the AD- and MQ-GST-326, as well as with C- and RC-GST-326 are not identical. If one compares panels 1 and 2 in Figure 4, it can be seen that the antenna array resonance positions of the arrays with MQ-GST-326 covering the antennas are shifted to slightly higher wavenumbers relative to the resonance positions of the arrays with AD-GST-326 as cover layer. If these shifts would origin from a shortening of the nanoantennas, they would correspond to a difference in antenna length ΔL of about 17 nm. Although scanning electron microscope (SEM) images do not show any damage of the antennas, a change of the antenna length of less than 20 nm can not be excluded due to the limited resolution of the SEM employed here.

Also, the antenna resonance positions of RC- and C-GST-326 differ for both antenna lengths, as can be seen, for example, in Figure 4, panel 3, marked resonance positions 2 and 4. If this difference of about 225 cm^{-1} (L = 500 nm) and about 245 cm^{-1} (L = 400 nm) would be related to a change in the antenna length, ΔL, the nanorods would need to shrink by about 36 nm. Since we would be able to image this decrease of the antenna length with our SEM, we can exclude it as the only reason for the difference in the reasonance position between the antenna array with C- and RC-GST-326 as cover layer. For sample layouts with antennas placed in between the GST-326 thin film, as well as with antennas placed on top of them, we noticed damaging of the antennas.

However, a possible explanation could be an incomplete phase-transition from MQ- to RC-GST-326, which would lead to a smaller refractive index relative to a fully crystallized GST-326 cover layer. This incomplete phase transition can be understood as a mixture of both phases (MQ- and RC-GST-326), resulting in an effective refractive index smaller than 6.33 (for crystalline GST-326 in the mid-IR). Since in Figure 3 C- and RC-GST-326 thin films show nearly identical reflectance behavior in the spectral range of the antenna arrays (2000–3000 cm^{-1}), we can attribute this incomplete phase transition to the presence of the antenna arrays.

For amorphous GST-326, the presence of the antennas leads to a 14% increase in absorption at 800 nm wavelength (cf. SI, Figure S1). The antenna area (width w × length L, cf. Figure 1B) is equal to about 4.2% of the total two-dimensional unit cell area (d_C^2, cf. Figure 1B). This leads to a 4.5-fold increase of the absorption in the amorphous GST-326 layer right on top of the antennas. In addition, the reflectance spectra (cf. SI, Figure S3A) show a slight decrease of the amorphous GST-326 with antennas relative to the thin films without antennas. If we compare the calculated absorption of the crystalline GST-326 thin film with and without antennas at the wavelength of the fs laser, an increase of less than 3% can be determined (cf. SI, Figure S2). Following the calculation above, this corresponds to a 1.7-fold increase of absorption only. Correspondingly, with antennas the reflectance (cf. SI, Figure S3B) increases slightly compared to the bare crystalline GST-326 thin film. Furthermore, this interpretation is supported by the calculated electromagnetic loss per volume displayed in Figure 5. There the loss in the GST-326 strongly increases, where the thin film directly covers the antenna. The high absorption in the amorphous GST-326 on top of the antennas could lead to melting of the GST-326 in the vicinity of the antennas after interacting with the optical pulses. The GST-326 is finally melt-

dx.doi.org/10.1021/ph500121d | ACS Photonics 2014, 1, 833–839

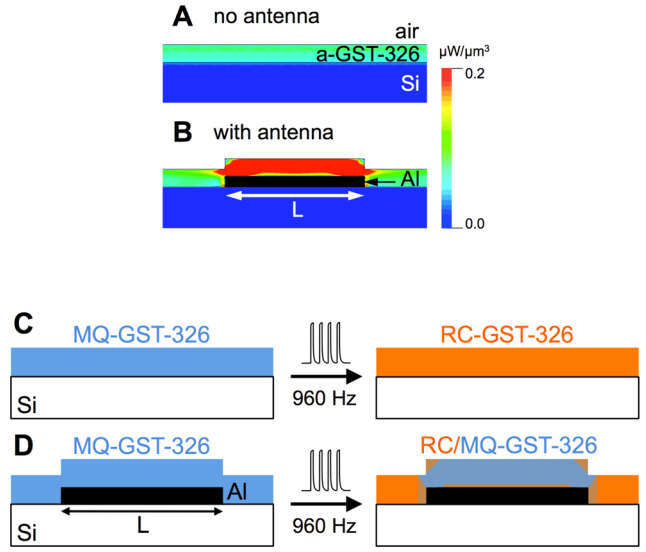

Figure 5. (A, B) Calculated total electromagnetic loss per volume in $\mu W/\mu m^3$ for the amorphous GST-326 thin film (A) and for the amorphous thin film covering an aluminum antenna (B). The presence of the antenna leads to a strongly enhanced absorbed energy in the GST-326 layer above the antenna. (C, D) Sample scheme before and after the fs laser pulse sequence for the GST-326 thin film (C) and for the GST-326 thin film with antenna (D). Due to the enhanced absorption in the amorphous GST-326 on top of the antenna, the MQ-GST-326, which directly covers the antenna, is partly melt-quenched again. In the area where no antenna is present the phase of the GST-326 is changed from MQ to RC, similar to the switching of the thin film (C). The color scale only belongs to (A) and (B).

quenched by thermal transport to the substrate and transforms the material on top of the antennas to the MQ phase, whereas the MQ-GST-326 thin film without antennas is fully recrystallized into RC-GST-326 (cf. SI, Figure S3).

In conclusion, we have demonstrated reversible switching of infrared antenna array resonances using fs laser-induced switching of the nonvolatile structural state of the PCM GST-326. We have introduced a simple and extremely thin sample geometry without the need for thermal barriers. The optical excitation allows to address single antenna arrays to switch them independently. These findings could lead to innovative applications in the field of active plasmonics, reconfigurable metamaterials, and switchable metasurfaces.[1,4,44]

The demonstrated reversible optical switching could also be extended to electrical switching, which is already realized in phase-change random access memories (PCRAMs).[32]

For future experiments, a parameter study (laser pulse energy, pulse repetition rate for crystallization) would be interesting to achieve maximum resonance frequency shifts and a high number of switching cycles. To achieve a better spatial resolution of the local switching behavior of the PCM in the vicinity of the antennas, the investigation with scanning nearfield optical microscopy (SNOM) would be very promising. This technique has been shown to allow imaging of single nanoantennas,[45] as well as the characterization of spatial domains, for example, of vanadium dioxide.[46] Pump–probe experiments[43,47] would allow to investigate the switching of resonance spectra with high temporal resolution. The sample geometry shown, which avoids capping layers, could facilitate the use of the characterization techniques mentioned above.

METHODS

Sample Preparation. For nanostructuring, electron beam lithography with a positive poly(methyl methacrylate)-based photoresist (thickness: 230 nm) has been used. After patterning, the samples were rinsed with developer and isopropyl alcohol. Thereafter, the metal layers, about 3 nm of chromium and about 32 nm of aluminum, have been deposited by thermal evaporation with rates of about 0.8 Å/s for chromium and 2.2 Å/s for aluminum as measured with a quartz crystal microbalance. Excess material was removed via lift-off in 60 °C warm acetone and the sample was rinsed in isopropyl alcohol and dried with nitrogen. After the nanoantenna arrays had been fabricated, the 50 nm GST-326 film has been direct current magnetron sputter-deposited with a background pressure of 2×10^{-6} mbar and 20 SCCM Ar flow.

Femtosecond Laser Source. The femtosecond laser source provides a beam with 800 nm (12500 cm^{-1}) central wavelength (cf. SI, Figure S1). A sequential arrangement of a Ti:sapphire oscillator and a Ti:sapphire regenerative amplifier emits single pulses of energy 1.65 mJ and 50 fs duration. It can also be operated in a repetitive mode with repetition rates up to 960 Hz. The optical pulses are attenuated by a polarizing beam splitter and subsequently focused by a 400 mm focal length spherical lens. The total power of the laser at a given repetition rate was measured with a calibrated power meter behind the focal spot. An *xyz*-translation stage at the focal spot was employed to position the sample as well as to scan a knife edge through the focal spot in order to determine the laser fluence at the position of the sample as a function of the transmission through the polarizing beam splitter. A Gaussian beam profile with full-width half-maximum of 230–270 μm was recorded at the position of the translation stage. The 800 nm light incident on the GST-326 sample is attenuated to $1/e$ of its incoming intensity after passing through 15 nm of crystalline or 56 nm of amorphous material.

Fourier Transform Infrared Spectroscopy. The Fourier transform infrared (FTIR) spectroscopy data have been collected averaging over 200 scans and 4 cm^{-1} resolution using a Bruker Vertex 70 interferometer coupled to a Bruker Hyperion microscope. All spectra have been collected in reflection mode using a 36-fold Cassegrain objective with an angle of incidence of about 25°. A variable knife-edge aperture of about (20×20) μm^2 defined the sample collection area. For spectra of the antenna arrays the background has been collected from an adjacent area with no antennas present. The spectra of the GST-326 thin films have been normalized to those of a gold mirror. The incident light is polarized along the antennas.

Calculation of the Total Electromagnetic Loss Per Volume. Calculations have been performed using the finite integration method (CST Microwave Studio) based on the dielectric permittivity data measured on thin film samples. In numerical simulations periodic boundary conditions have been used in the transverse direction. In the vertical direction the simulation domain has been terminated using perfectly matched layer (PML) boundary conditions. Plane wave excitation in combination with the Floquet Modes Port has been employed.

ASSOCIATED CONTENT

Supporting Information

Normalized absorption and reflectance spectra of amorphous and crystalline GST-326 with and without antennas are

dx.doi.org/10.1021/ph500121d | ACS Photonics 2014, 1, 833–839

depicted in Figures S1−S3. This material is available free of charge via the Internet at http://pubs.acs.org.

AUTHOR INFORMATION

Corresponding Author

*E-mail: taubner@physik.rwth-aachen.de.

Notes

The authors declare no competing financial interest.

ACKNOWLEDGMENTS

A.U.M. wishes to thank Martin Reininghaus and Tobias Maß for helpful discussions, Lena Jung and Peter Lingnau for technical assistance, and especially Prof. Mark Brongersma at Stanford University for granting access to his laboratory. This work was supported by the DFG under SFB 917, the Excellence Initiative of the German federal and state governments and the Ministry of Innovation of North-Rhine-Westphalia. P.Z. acknowledges funding from the Humboldt foundation. A.M.L. acknowledges support from the U.S. Department of Energy, Office of Science, Basic Energy Sciences.

REFERENCES

(1) Kildishev, A.; Boltasseva, A.; Shalaev, V. M. Planar photonics with metasurfaces. *Science* **2013**, *339* (6125), 1232009(1)−1232009(6).

(2) Gordon, J. A.; Holloway, C. L.; Booth, J.; Kim, S.; Wang, Y.; Baker-Jarvis, J.; Novotny, D. R. Fluid interactions with metasurfaces for tuning, sensing and microwave-assisted chemical processess. *Phys. Rev. B* **2011**, *83* (20), 205130(1)−205130(5).

(3) Fan, P.; Chettiar, U. K.; Cao, L.; Afshinmanesh, F.; Engheta, N.; Brongersma, M. L. An invisible metal-semiconductor photodetector. *Nat. Photonics* **2012**, *6* (6), 380−385.

(4) Zheludev, N. I.; Kivshar, Y. S. From metamaterials to metadevices. *Nat. Mater.* **2012**, *11* (11), 917−924.

(5) Pryce, I. M.; Aydin, K.; Kelaita, Y.; Briggs, R. M.; Atwater, H. A. Highly strained compliant optical metamaterials with large frequency tunability. *Nano Lett.* **2010**, *10* (10), 4222−4227.

(6) Driscoll, T.; Kim, H.-T.; Chae, B.-G.; Kim, B.-J.; Lee, Y.-W.; Jokerst, N. M.; Palit, S.; Smith, D. R.; Di Ventra, M.; Basov, D. N. Memory metamaterials. *Science* **2009**, *325* (5947), 1518−1521.

(7) Jun, Y. C.; Reno, J.; Ribaudo, T.; Shaner, E.; Greffet, J.-J.; Vassant, S.; Marquier, F.; Sinclair, M.; Brener, I. Epsilon-near-zero strong coupling in metamaterial-semiconductor hybrid structures. *Nano Lett.* **2013**, *13* (11), 5391−5396.

(8) Decker, M.; Kremers, C.; Minovich, A.; Staude, I.; Miroshnichenko, A. E.; Chigrin, D.; Neshev, D. N.; Jagadish, C.; Kivshar, Y. Electro-optical switching by liquid-crystal controlled metasurfaces. *Opt. Exp.* **2013**, *21* (7), 8879−8885.

(9) Miao, X.; Passmore, B.; Gin, A.; Langston, W.; Vangala, S.; Goodhue, W.; Shaner, E.; Brener, I. Doping tunable resonances: Toward electrically tunable mid-infrared metamaterials. *Appl. Phys. Lett.* **2010**, *96* (10), 101111(1)−101111(3).

(10) Yao, Y.; Kats, M. A.; Genevet, P.; Yu, N.; Song, Y.; Kong, J.; Capasso, F. Broad electrical tuning of graphene-loaded plasmonic antennas. *Nano Lett.* **2013**, *13* (3), 1257−1264.

(11) Dicken, M. J.; Aydin, K.; Pryce, I. M.; Sweatlock, L. A.; Boyd, E. M.; Walavalkar, S.; Ma, J.; Atwater, H. A. Frequency tunable near-infrared metamaterials based on VO_2 phase transition. *Opt. Exp.* **2009**, *17* (20), 18330−18339.

(12) Liu, N.; Tang, M. L.; Hentschel, M.; Giessen, H.; Alivisatos, A. P. Nanoantenna-enhanced gas sensing in a single tailored nanofocus. *Nat. Mater.* **2011**, *10* (8), 631−636.

(13) Tittl, A.; Mai, P.; Taubert, R.; Dregely, D.; Liu, N.; Giessen, H. Palladium-based plasmonic perfect absorber in the visible wavelength range and its application to hydrogen sensing. *Nano Lett.* **2011**, *11* (10), 4366−4369.

(14) Strohfeldt, N.; Tittl, A.; Schäferling, M.; Neubrech, F.; Kreibig, U.; Griessen, R.; Giessen, H. Yttrium hydride nanoantennas for active plasmonics. *Nano Lett.* **2014**, *14* (3), 1140−1147.

(15) Wuttig, M.; Yamada, N. Phase-change materials for rewriteable data storage. *Nat. Mater.* **2007**, *6* (11), 824−832.

(16) Lencer, D.; Salinga, M.; Grabowski, B.; Hickel, T.; Neugebauer, J.; Wuttig, M. A map for phase-change materials. *Nat. Mater.* **2008**, *7* (12), 972−977.

(17) Raoux, S.; Ielmini, D.; Wuttig, M.; Karpov, I. Phase-change materials. *MRS Bull.* **2012**, *37* (2), 118−123.

(18) Shportko, K.; Kremers, S.; Woda, M.; Lencer, D.; Robertson, J.; Wuttig, M. Resonant bonding in crystalline phase-change materials. *Nat. Mater.* **2008**, *7* (8), 653−658.

(19) Michel, A. U.; Chigrin, D. N.; Maß, T. W. W.; Schönauer, K.; Salinga, M.; Wuttig, M.; Taubner, T. Using low-loss phase-change materials for mid-infrared antenna resonance tuning. *Nano Lett.* **2013**, *13* (8), 3470−3475.

(20) Sámson, Z. L.; MacDonald, K. F.; De Angelis, F.; Gholipour, B.; Knight, K.; Huang, C. C.; Di Fabrizio, E.; Hewak, D. W.; Zheludev, N. I. Metamaterial electro-optic switch of nanoscale thickness. *Appl. Phys. Lett.* **2010**, *96* (14), 143105(1)−143105(3).

(21) Pernice, W. H. P.; Bhaskaran, H. Photonic non-volatile memories using phase-change materials. *Appl. Phys. Lett.* **2012**, *101* (17), 171101(1)−171101(4).

(22) Rudé, M.; Pello, J.; Simpson, R. E.; Osmond, J.; Roelkens, G.; van der Tol, J. J. G. M.; Pruneri, V. Optical switching at 1.55 μm in silicon racetrack resonators using phase change materials. *Appl. Phys. Lett.* **2013**, *103* (14), 141119(1)−141119(4).

(23) Cao, T.; Zhang, L.; Simpson, R. E.; Cryan, M. J. Mid-infrared tunable polarization-independent perfect absorber using a phase-change metamaterial. *J. Opt. Soc. Am. B* **2013**, *30* (6), 1580−1585.

(24) Cao, T.; Wei, C.; Simpson, R. E.; Zhang, L.; Cryan, M. J. Fast tuning of double fano resonance using a phase-change metamaterial under low power intensity. *Sci. Rep.* **2014**, *4* (4463), 1−9.

(25) Cao, T.; Zhang, L.; Simpson, R. E.; Wei, C.; Cryan, M. J. Strongly tunable circular dichroism in gammadion chiral phase-change metamaterials. *Opt. Express* **2013**, *21* (23), 27841−27851.

(26) Hira, T.; Homma, T.; Uchiyama, T.; Kuwamura, K.; Saiki, T. Switching of localized surface plasmon resonance of gold nanoparticles on a GeSbTe film mediated by nanoscale phase change and modification of surface morphology. *Appl. Phys. Lett.* **2013**, *103* (24), 241101(1)−241101(4).

(27) Matsunaga, T.; Kojima, R.; Yamada, N.; Kifune, K.; Kubota, Y.; Takata, M. Structural investigation of $Ge_3Sb_2Te_6$, an intermetallic compound in GeTe-Sb_2Te_3 homologous series. *Appl. Phys. Lett.* **2007**, *90* (16), 161919(1)−161919(3).

(28) Kats, M. A.; Blanchard, R.; Genevet, P.; Yang, Z.; Qazilbash, M. M.; Basov, D. N.; Ramanathan, S.; Capasso, F. Thermal tuning of mid-infrared plasmonic antenna arrays using a phase change material. *Opt. Lett.* **2013**, *38* (3), 368−370.

(29) Wang, W. J.; Shi, L. P.; Zhao, R.; Lim, K. G.; Lee, H. K.; Chong, T. C.; Wu, Y. H. Fast phase transitions induced by picosecond electrical pulses on phase change memory cells. *Appl. Phys. Lett.* **2008**, *93* (4), 043121(1)−043121(3).

(30) Salinga, M.; Carria, E.; Kaldenbach, A.; Bornhöfft, M.; Benke, J.; Mayer, J.; Wuttig, M. Measurement of crystal growth velocity in a melt-quenched phase-change material. *Nat. Commun.* **2013**, *4* (2371), 1−8.

(31) Iwasaki, H.; Harigaya, M.; Nonoyama, O.; Kageyama, Y.; Takahashi, M.; Yamada, K.; Deguchi, H.; Ide, Y. Completely erasable phase change optical disc II: application of Ag-In-Sb-Te mixed-phase system for rewritable compact disc compatible with cd-velocity and double cd-velocity. *Jpn. J. Appl. Phys.* **1993**, *32* (11), 5241−5247.

(32) Kwon, Y.; Kim, J.; Chae, S.; Lee, Y.; Kim, S. G.; Ku, J.; Sohn, Y.; Park, S. J. Device characteristics of a Ge-doped SbTe alloy for high-speed phase-change random access memory. *Korean Phys. Soc.* **2011**, *59* (2), 466−469.

(33) Gholipour, B.; Zhang, J.; MacDonald, K. F.; Hewak, D. W.; Zheludev, N. I. An all-optical, non-volatile, bidirectional, phase-change meta-switch. *Adv. Mater.* **2013**, *25* (22), 3050−3054.
(34) Pandian, R.; Kooi, B. J.; De Hosson, J. T. M. Influence of capping layers on the crystallization of doped Sb_xTe fast-growth phase-change films. *J. Appl. Phys.* **2006**, *100* (12), 123511(1)−123511(9).
(35) Sarrazin, M.; Vigneron, J.-P.; Vigoureux, J.-M. Role of wood anomalies in optical properties of thin metallic films with a bidimensional array of subwavelength holes. *Phys. Rev. B* **2003**, *67* (8), 085415(1)−085415(8).
(36) Boyen, H.-G.; Cossy-Favre, A.; Oelhafen, P.; Siber, A.; Ziemann, P.; Lauinger, C.; Moser, T.; Haussler, P.; Baumann, F. Low-temperature interface reactions in layered Au/Sb films: In situ investigation of the formation of an amorphous phase. *Phys. Rev. B* **1995**, *51* (3), 1791−1802.
(37) Johnson, N. P.; Khokhar, A. Z.; Chong, H. M. H.; De La Rue, R. M.; McMeekin, S. Characterisation at infrared wavelengths of metamaterials formed by thin-film metallic split-ring resonator arrays on silicon. *Electron. Lett.* **2006**, *42* (19), 1−2.
(38) Kremers, S. Optische Eigenschaften von Phasenwechselmaterialien für zukünftige optische und elektronische Speicheranwendungen. *Ph.D. Thesis*, RWTH Aachen University, Aachen, Germany, 2009.
(39) Salinga, M.; Wuttig, M. Phase-change memories on a diet. *Science* **2011**, *332*, 543−544.
(40) Abrikosov, N. K.; Dinalova-Dobryakova, G. T. An investigation of the structural diagram of Sb_2Te_3-GeTe. *Izv. Akad. Nauk S.S.S.R. Neorg. Mater.* **1965**, *1* (2), 204−207.
(41) Sittner, E.-R.; Siegert, K. S.; Jost, P.; Schlockermann, C.; Lange, F. R. L.; Wuttig, M. $(GeTe)_x$-$(Sb_2Te_3)_{1-x}$ phase-change thin films as potential thermoelectric materials. *Phys. Status Solidi A* **2013**, *210* (1), 147−152.
(42) Cotton, R. L.; Siegel, J. Stimulated crystallization of melt-quenched $Ge_2Sb_2Te_5$ films employing femtosecond laser double pulses. *J. Appl. Phys.* **2012**, *112* (12), 123520(1)−123520(5).
(43) Sokolowski-Tinten, K.; Solis, J.; Bialkowski, J.; Siegel, J.; Afonso, C. N.; von der Linde, D. Dynamics of ultrafast phase changes in amorphous GeSb films. *Phys. Rev. Lett.* **1998**, *81* (17), 3679−3682.
(44) Ou, J. Y.; Plum, E.; Jiang, L.; Zheludev, N. I. Reconfigurable photonic metamaterials. *Nano Lett.* **2011**, *11* (5), 2142−2144.
(45) Hoffmann, J. M.; Hauer, B.; Taubner, T. Antenna-enhanced infrared near-field nanospectroscopy of a polymer. *Appl. Phys. Lett.* **2012**, *101* (19), 193105(1)−193105(4).
(46) Jones, A. C.; Berweger, S.; Wei, J.; Cobden, D.; Raschke, M. B. Nano-optical investigations of the metal-insulator phase behavior of individual VO_2 microcrystals. *Nano Lett.* **2010**, *10* (5), 1574−1581.
(47) Kübler, C.; Ehrke, H.; Huber, R.; Lopez, R.; Halabica, A.; Haglund, R. F., Jr.; Leitenstorfer, A. Coherent structural dynamics and electronic correlations during an ultrafast insulator-to-metal phase transition in VO_2. *Phys. Rev. Lett.* **2007**, *99* (11), 116401(1)−116401(4).